Journal of Saudi Chemical Society (2014) **18**, 169–182

King Saud University

Journal of Saudi Chemical Society

www.ksu.edu.sa
www.sciencedirect.com

ORIGINAL ARTICLE

Passivity characteristics on Ni(Cr)(Fe)SiB glassy alloys in phosphate solution

Sanaa T. Arab [a,*], Khadijah M. Emran [b], Hamad A. Al-Turaif [c]

[a] *Department of Chemistry, Sciences Faculty for Girls, King Abdulaziz University, P.O. Box 2321, Jeddah 21451, Saudi Arabia*
[b] *Department of Applied Chemistry, College of Applied Science, Taibah University Al-Madinah Al-Monawarah, Saudi Arabia*
[c] *Department of Chemical and Materials Engineering, King Abdulaziz University, Jeddah, Saudi Arabia*

Received 12 February 2011; accepted 18 May 2011
Available online 12 June 2011

KEYWORDS

Metallic glasses;
Passivity;
Hydrated chromium oxyhydroxide;
Spontaneous passivation;
Polarization;
EIS;
XPS;
SEM

Abstract Passivity characteristics of three nickel-metalloids glassy alloys ($Ni_{92.3}Si_{4.5}B_{32}$, $Ni_{82.3}Cr_{7}Fe_3Si_{4.5}B_{3.2}$ and $Ni_{75.5}Cr_{13}Fe_{4.2}Si_{4.5}B_{2.8}$) and the immersion time effect on the corrosion resistance were carried out by AC and DC electrochemical methods and SEM and XPS analyses. The study also focused on the effect of H_3PO_4 concentration and its role on the corrosion rate, passivation ability of nickel base glassy alloys surface. The present investigation revealed (i) corrosion resistance of Cr-free alloy shows pseudo passivity at all examined H_3PO_4 concentrations, (ii) high corrosion resistance of Cr contains alloys due to the formation of protective layer of chromium oxyhydroxide on the surface which acts as a diffusion barrier against alloy dissolution, (iii) the negative resistance observed in the case $Ni_{75.5}Cr_{13}Fe_{4.2}Si_{4.5}B_{2.8}$ alloy revealed the sudden transition of metal/solution interface from a state of active dissolution to the passive state.

1. Introduction

Many new materials have emerged in last 30 years: amorphous metal ribbons, glass fibers, high temperature superconductors, quasicrystals, bulk metallic glasses (BMGs) and metal foams. Their novel structures promise and, in many cases, do deliver novel properties, or rather the combinations of properties, which make them attractive for applications (Inoue, 1998; Johnson, 1999; Salimon et al., 2004).

The high corrosion resistance of metallic amorphous is due to their structure which is chemically homogeneous, so they have no crystallographic dislocations, crystal imperfections, distortions, grain boundaries or secondary phase elements, and therefore the passive films on these surfaces are more uniform and stable than films on conventional crystalline surfaces (Asami et al., 1976).

* Corresponding author. Tel.: +699505600455; fax: +69926622071.
E-mail addresses: prof.s.t.arab@hotmail.com (S.T. Arab), k_imran2000sa@yahoo.co.uk (K.M. Emran), hturaif@kau.edu.sa (H.A. Al-Turaif).

Peer review under responsibility of King Saud University.
doi:10.1016/j.jscs.2011.05.020

Production and hosting by Elsevier

In the context of corrosion, passivation is the spontaneous formation of a hard non-reactive surface film that inhibits further corrosion. This layer is usually an oxide or nitride which is a few atoms thick (http://en.wikipedia.org/wiki/Passivation).

The high corrosion resistance of the chromium valve metal alloys results from the formation of protective thin surface which leads to spontaneous passivation of these alloys. For a better understanding of the extremely high corrosion resistance of these alloys, it is necessary to characterize the composition and in depth distribution of the passive layer as well as their s composition and existence during immersion in phosphoric acid (Oelhafen et al., 1979).

It is well known that chromium forms a highly protective passive film in less oxidizing environments but dissolves transpassivity at high anodic potentials. Surface analysis methods such as X-ray photoelectron spectroscopy "XPS" has been used for the study of the passive film on metallic glasses alloys (Slemnik et al., 2002; Asami and Hashimoto, 1977; Kawashima et al., 1984; Zhang et al., 1992a,b; Lee et al., 1997; Katagiri et al., 2001; Wu et al., 2006; Qin et al., 2010a,b).

The aim of this work is the study of the concentration effect of phosphoric acid in the range 1–12 M, at 30 °C on the passivation of nickel-metalloids glassy alloys: ($Ni_{92.3}Si_{4.5}B_{32}$, $Ni_{82.3}Cr_7Fe_3Si_{4.5}B_{3.2}$ and $Ni_{75.5}Cr_{13}Fe_{4.2}Si_{4.5}B_{2.8}$) The anodic passivation is to reinforce the film spontaneously formed for 15 min of immersion; the study of passivation is conducted by potentiodynamic polarization followed by electrochemical impedance spectroscopy (EIS) measurements. The passivity formation was estimated in 3 M H_3PO_4 at different immersion times.

2. Experimental

2.1. Specimens and test solutions

Ingot $Ni_{92.3}Si_{4.5}B_{32}$, $Ni_{82,3}Cr_7Fe_3Si_{4.5}B_{3.2}$ and $Ni_{75.5}Cr_{13}Fe_{4.2}Si_{4.5}B_{2.8}$ (at%) alloys were supplied by Vacuumschmelze with physical properties summarized in Table 1. Rounded specimens were cut from a foil (2.5–7.5 mm width and 20–50 μm thickness) with a working area of (2.4 mm^2).

Each experiment was carried out with a new strip. The electrodes were decreased with alcohol and rinsed several times with double distilled water and finally cleaned in an ultrasonic bath. The electrodes were connected to a copper specimen holder and immersed in the test solution without drying.

Aerated solutions of H_3PO_4 (Panreac) were used as corrosion medium. Appropriate concentrations of the acid were prepared by dilution using double distilled water.

2.2. Methods

Electrochemical measurements have been achieved by connecting the electrochemical cell to ACM Gill AC instrument and to a Samsung computer (Bridge DVD ASUS 8× max). In the conventional cell three-electrode assembly, containing naturally aerated H_3PO_4 solutions, the working electrode was nickel-base glassy alloy (2.4 mm^2), Table 1, platinum wire and saturated calomel electrodes were used as counter and reference electrodes, respectively. Experiments were carried out in stagnant solutions at 30 °C ± 1.

After immersion of the specimen, prior to the impedance measurement, a stabilization period of 15 min was found, which is sufficient for E_{ss} (the steady-state potential) to be established. The AC frequency range extended from 30 kHz to 0.1 Hz, a 10 mV peak to peak sine wave being the excitation signal. The impedance spectra were fitted using a non-linear least-squares fitting procedure developed by Boukamp (Macdonald and Johanson, 1987).

The Nyquist diagrams were characterized by depressed capacitive loops with the theoretical center located below the real axis (Fig. 1), so, the measured capacitive response is not generally ideal (i.e., a pure capacitor).

A constant phase element (CPE) is then introduced for the spectra fitting, instead of an ideal capacitance element. The impedance expression of CPE is given by:

$$Z_{CPE} = \frac{1}{Q(j\omega)^n} \quad (1)$$

where Q and n are frequency-independent fit parameters, $j = (-1)^{1/2}$ the imaginary number and $\omega = 2nf$ the angular frequency in radius. The factor n, the CPE exponent, is an adjustable parameter.

For $n = 1$ the CPE describes an ideal capacitor with Q (mF/cm^2) equal to the capacitance C and the phase angle Θ equal to 90° and for $n = 0$ the CPE is an ideal resistor and the phase angle equal to 0°. When $n = 0.5$ the CPE represents a Warburg impedance with diffusion character and for $0.5 < n < 1$ the CPE describes a frequency dispersion of time constant due to local inhomogeneties in the dielectric material. Inductance characteristics presents when $n = -1$. In general, it is believed that the CPE is related to some type of heterogeneity of the electrode surface as well as to the fractal nature (roughness or porosity) of the surface (Macdonald and Johanson, 1987).

Analysis of the impedance spectra was done by fitting the experimental data to equivalent circuit. The quality of fitting to the equivalent circuit (EC) was judged firstly by the Chi-square (χ^2) values and secondly by the error distribution versus frequency, comparing experimental with simulated data.

Potentiodynamic polarization curves were obtained with a potential sweep rate of 1 mV/s. The potential was sweep from cathodic to anodic directions after impedance run. Corrosion current densities (I_{corr}) were calculated by extrapolating the Tafel lines to corrosion potential (E_{corr}). Passivation parameters: critical passivation current density (I_{cc}), critical passivation potential (E_{cc}), passivation potential (E_{pass}), passivation

Table 1 Some physical properties of studied alloys.

Specimens	Alloy composition (electrode)	Melting temperature (°C)	Density (gm/cm^3)
I	$Ni_{92.3}Si_{4.5}B_{3.2}$	1054	8.07
II	$Ni_{82.3}Cr_7Fe_3Si_{4.5}B_{3.2}$	1024	7.88
III	$Ni_{75.5}Cr_{13}Fe_{4.2}Si_{4.5}B_{2.8}$	1103	7.82

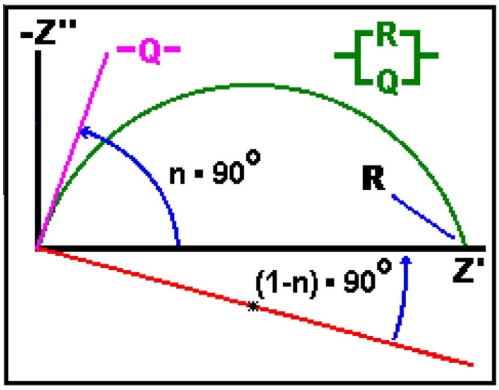

Figure 1 The Nyquist (Complex Impedance Plane) Plot of a CPE is a simple one. For a solitary CPE (symbolized here by Q), it is just a straight line which makes an angle of $(n \times 90°)$ with the x-axis as shown in pink in the figure. The plot for a resistor (symbolized by R) in parallel with a CPE is shown in green. In this case the center of the semicircle is depressed by an angle of $(1 - n) \times 90°$.

current density (I_{pass}) were determined from the potentiodynamic polarization curves. Cyclic polarization curves were used to reveal the stability of the passive film at different immersion times. To assess the susceptibility of passive film on nickel base glassy alloy, cyclic polarization curves were used.

After the electrochemical test in 3.0 M H_3PO_4, the chemical compositions of the alloy surface were detected by XPS using a multi-technique surface analysis system (MAX200, Leybold) with MgKα and AlKα at 100 W of X-ray power. The pressure in the analysis chamber during sample analysis was less than 10^{-8} m bar.

The nickel base specimens coated by a film of 50 nm of gold by sputtering, have been investigated by using a XL20-PHILIPS SEM. The data obtained from these experimental methods were compared.

3. Results and discussion

3.1. Effect of acid

3.1.1. AC electrochemical results

The impedance is one of most relevant quantities that can be measured in electrochemistry and corrosion. Many corrosion processes are controlled kinetically by the charge transfer at the interface and/or by the transport of a reactant to, or a product from the surface and have a profound effect on the rates of corrosion of metals. Both processes have been studied extensively using EIS. The analysis of mechanisms for corrosion of iron and other metals in aqueous solutions and also the identification of the elementary steps involved in active dissolution, active–passive transitions and passivation of metals have been studied with EIS.

Fig. 2a and b show the Nyquist plots for alloy I (Cr-free) in H_3PO_4 acid in the range 1.0–12.0 M. The plots exhibit single capacitive loop regardless of PO_4^{3-} concentration. This means that the corrosion process occurs in one step.

As can be observed that, at low concentrations 1.0–3.0 M of H_3PO_4, the obtained diameter of the capacitive loop is decreased. The spectra were found to fit the equivalent circuit (EC) shown in Scheme 1 with the circuit description code (CDC) R(RQ). Farther increase in $[H_3PO_4]$, in the range 6.0–12.0 M, increases the diameter of capacitive arc (increase in R_{ct} values and decrease Q values, Table 2) is found. Bode plots shown in Fig. 2b exhibit single tine constant. The maximum phase angle Θ_{max} is approached to 90° with long relaxation time (a broad peak) shifted to low frequency. The single peaks observed corresponded to the alloy/electrolyte interface. The diagrams at 6.0 M and 9.0 M of H_2PO_4 which show capacitance are at high and intermediate frequencies range followed by a tail at lower frequencies. The capacitive arc may be related with the dielectric properties of the formed film on the electrode surface at the open circuit potential but it may be also related to the electric double layer capacitance at the electrode/solution interface, which includes a metal/film interface followed by a film/solution interface. The tail is probably associated with the mass transport process in the solution. Several models of equivalent circuits were attempted to fit these experimental data. The best agreement between experiment and fitting was obtained with the equivalent circuit of Scheme 2 with circuit description code (CDC) for as R(Q(RW)).

The Warburg impedance $Z\omega$ can be presented as (Chen et al., 2000; Arab and Emran, 2009):

$$Z\omega = \sigma\omega^{-1/2}(1 - j) \tag{2}$$

where, a is the Warburg coefficient ($\Omega\,cm^2\,s^{-1/2}$).

The model as shown in Scheme 2 includes two parallel resistance and capacitance combinations and Warburg impedance, which are considered to contain coating film, metal substrate and diffusion information.

The total impedance value can be presented as:

$$Z_{total} = R_s + R_{ct} + -\sigma\omega^{-1/2} - \sigma\omega^{-1/2}\mathrm{j} \tag{3}$$

$$Z_{total} = R_s + R_{ct} + Z_\omega \tag{4}$$

From Eq. (2), the imaginary portion, $(-\sigma\omega^{-1/2})$, only represents the information of the diffusion process. Therefore in the Nyquist plots at low frequency, where the diffusion tail shows up, the value of Imag-axis presents the item of $\sigma\omega^{-1/2}$. The modulus of Warburg impedance:

$$lZwl = \sqrt{2}\sigma\omega^{-1/2} \tag{5}$$

so, Warburg impedance can be obtained by the value of Imag-axis at low frequency. b_f is defined by the following equation:

$$b_f = -\sigma\omega^{-1/2} \tag{6}$$

The large value of b_f, indicates the more difficult for the ions to diffuse through the pores within the formed passive films.

The value of b_f corresponding to the low frequency increases with $[H_3PO_4]$ increase. This implies that the passive film on the metal surface become less porous with the increase of the phosphate concentration and leads to lower corrosion rates so, the film will promote the alloy corrosion inhibition, as indicated by the disappearance of the inductive arc and by increasing of R_{ct} values when acid concentration increases. Value of R_{ct} obtained in 3.0 M of H_3PO_4 is lower about 26.8% from the value at 1.0 M, resulting increase in corrosion rate. But farther increase in $[H_3PO_4]$ increase R_{ct} value (it is high as about 60.7% from the value at 1.0 M) indicating the proved the corrosion resistance.

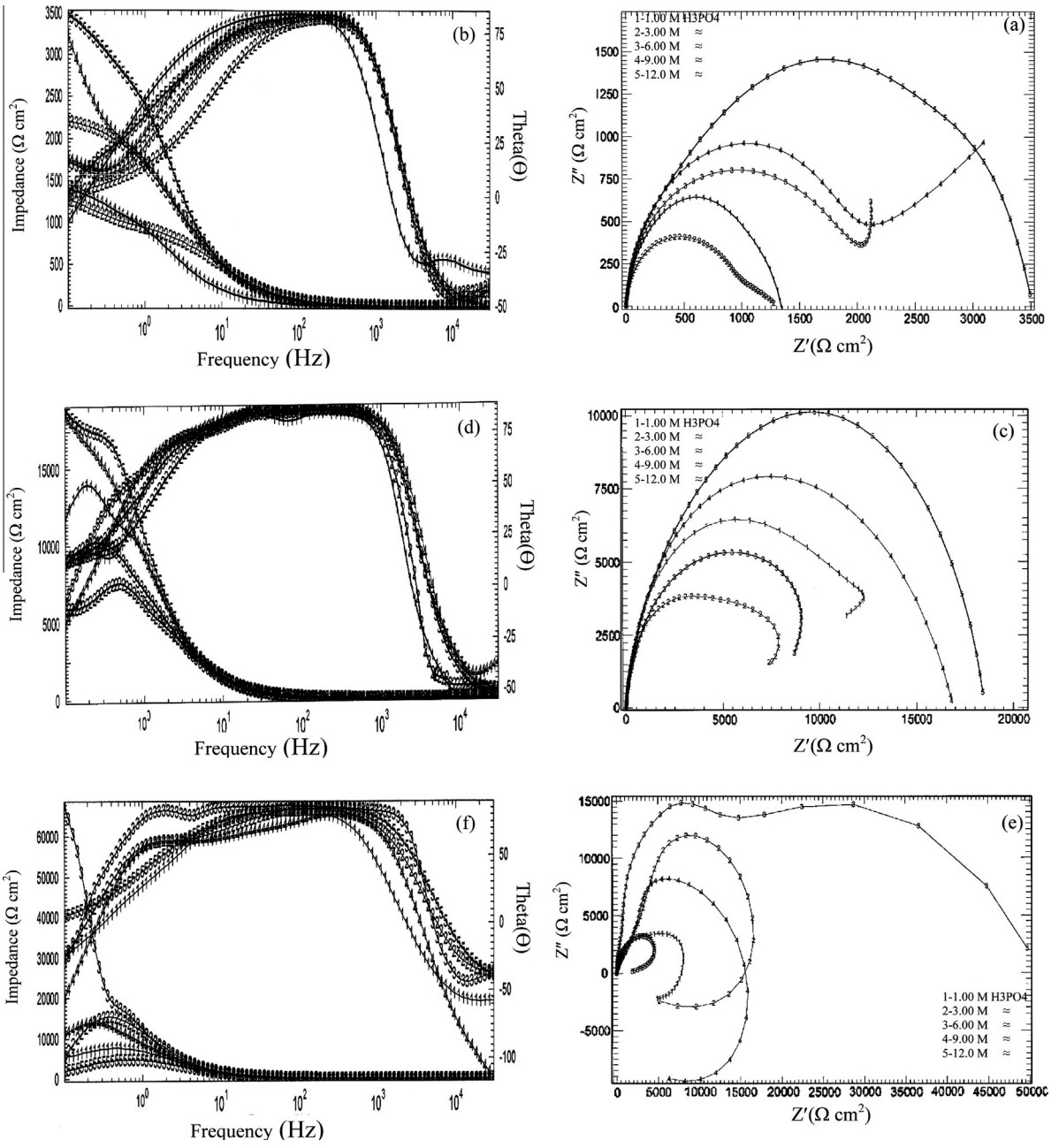

Figure 2 Impedance plots of metallic glassy alloys in different concentrations of H_3PO_4: (a) Nyquist plots, (b) Bode plots.

This process results in a noticeable decrease in CPE/C_{dl}, and the trend is in accordance with the Helmholtz model, is given by the following equation:

$$C_{dl} = \frac{\varepsilon\varepsilon^0 A}{d} \tag{7}$$

where d is the average thickness of the protective layer, ε is the dielectric constant of the medium, ε^0 is the vacuum permittivity ($\varepsilon_o = 8.854 \times 10^{-12}$ F m^{-1}) and A is the effective surface area of the electrode. The obtained results may interoperated due to the increase in the passive film formed on the alloy surface which becomes more thick. This protective film consists of two layers; the outer layer is porous where as the inner is a compact one, as shown in Scheme 3.

The diffusion tail disappeared at 12.0 M H_3PO_4 which may due to block of pores by increasing [PO_4^{3-}]. Similar behavior observed by alloy II in H_3PO_4 acid solution as shown in Fig. 2c and d. The diameter of capacitive arc is related to the electric double layer capacitance at the electrode/solution interface, which includes metal film interface followed by a film/solution interface decrease when the [H_3PO_4] increase from 1.0 to 3.0 M (inflection point). The opposite observations are recorded when the H_3PO_4 concentration increases up to 12.0 M. The alloy resistance increases by about 60.9% at 12.0 M H_3PO_4 than at 1.0 M as shown in Table 2.

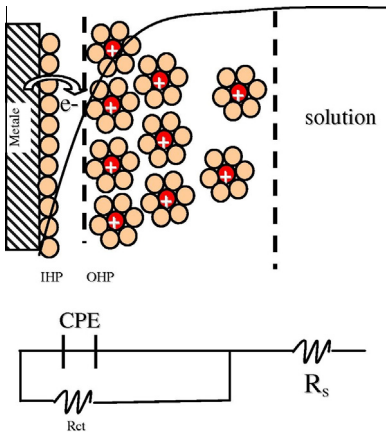

Scheme 1 Equivalent circuit for the metal–acid interface with a Faraday impedance R_{ct} equal to a resistance, Re is the electrolyte resistance, Q the capacity of double layer and R_{et} is the charge transfer resistance.

These figures show one well-defined open semicircle in the Nyquist plot, in range 1.0–6.0 M, followed by a pseudo inductive loop at low frequencies. The combination of a capacitive and a pseudo-inductive loop can be explained by the relaxations of the surface coverage's of two intermediate species, one of them accelerating the rate of the overall process in the film/solution region and the other decelerating it.

The maximum value in phase angel curve with the phase angle Θ_{max} close to 90°, suggests that the electrochemical process occurring at high frequency favors the formation of the protective film (Singh and Hosseini, 1993). The n values in Table 2 were close to 1 (~0.94) which indicates the behavior of an ideal capacitor. The one time-constant mechanism of the alloy II in high concentrations of H_3PO_4 revealed homogeneous corrosion process (charge transfer control). Pseudo-inductive loop at the end of the spectra denoting the ability of the oxide to reactivate and hilling the defect occur by PO_4^{3-} ion on the oxide layer. Increasing the dissolution resistance of the alloy II, may due to the filling the pores in the outer layer resulting in improvement of the passive state and decrease in CPE/Q values and corrosion rate mm/y.

The Nyquist plots of alloy III (Fig. 2e and f) at 1.0 M and 12.0 M H_3PO_4 are composed of one semicircle with the lower end crossing the real axis. Corresponding Bode plot of log f vs. phase angle (Θ) exhibited wide single peak indicating single time constant (one step). The single peaks observed correspond to the film/electrolyte interfacing. This system can be modeled as the Randle equivalent circuit Scheme 1. Two defined semicircles (two well resolved relaxation time constants) were observed at 6.0 M, where the spectra at 3.0 M and 9.0 M have low overlapped time constants so they not well visible. These EIS plots can be interpreted by using two time constants. The electrochemical parameters obtained from fitting the recorded EIS data using the equivalent circuits of Scheme 4. The CDC for the equivalent circuit proposed for this system is $R(Q[R(QR)])$. This equivalent circuit is relatively simple but accounts well for the presence of the two time constants in the impedance diagrams. R_e the electrolyte resistance, C_f the passive film capacity, R_p the electrolytic resistance in the defects of the passive film, C_{dl} the double layer capacity and R_{ct} is the charge transfer resistance. Fitting data to the suitable equivalent circuits are summarized in Table 2.

This model assumes that the passive film does not totally cover the metal and cannot be considered as a homogeneous layer but rather as a defective layer. In fact, neither real surfaces of solids in the active range nor passive films on metallic substrates can be considered to be ideally homogeneous. By analogy to the well-established model for the oxide film of the nickel base alloy, the high-frequency behavior can be attributed to the defective passive film and the low-frequency response to the anodic nickel dissolution reaction at the interface metal/solution at the bottom of the pores. The selection of this circuit was a compromise between a reasonable fitting of the experimental values and a minimum of components in the equivalent circuit.

The increase in CPE/Q is indicative to a surface roughness which increases the surface area. The value of exponent n (the degree of inhomogeneous) is in the range 0.90–0.97 which reveal the capacitive behavior of the oxide layer.

Table 2 Electrochemical kinetic parameters and corrosion rate obtained by EIS technique for Ni-base metallic glasses alloys in naturally aerated H_3PO_4 solutions at 30 °C.

Alloy	C_{HCL} (M)	R_{ct} (Ω cm^2)	CPE (Q) (μF/cm^2)	n	Corrosion rate (mm/y)
I	01.0	1378	48.52	0.93	0.36
	03.0	1009	49.96	0.96	0.49
	06.0	2100	48.17	0.91	0.23
	09.0	2182	47.41	0.92	0.22
	12.0	3503	45.12	0.87	0.14
II	01.0	11210	12.09	0.99	0.025
	03.0	7832	14.68	0.94	0.036
	06.0	11040	12.76	0.89	0.026
	09.0	16840	12.82	0.93	0.017
	12.0	18410	12.49	0.94	0.015
III	01.0	7615	11.39	0.96	37.3×10^{-3}
	03.0	14900	05.87	0.97	19.1×10^{-3}
	06.0	38030	01.22	0.97	5.72×10^{-3}
	09.0	13420	06.44	0.91	21.2×10^{-3}
	12.0	5093	17.53	0.94	55.8×10^{-3}

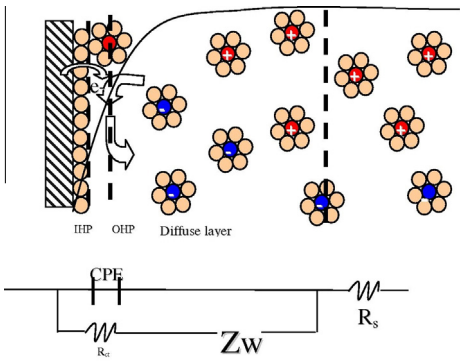

Scheme 2 Equivalent circuit model for the metal suffering localized attack. R_s, solution resistance; R_{ct}, charge transfer resistance; Q, double layer capacitance; W, Warburg impedance.

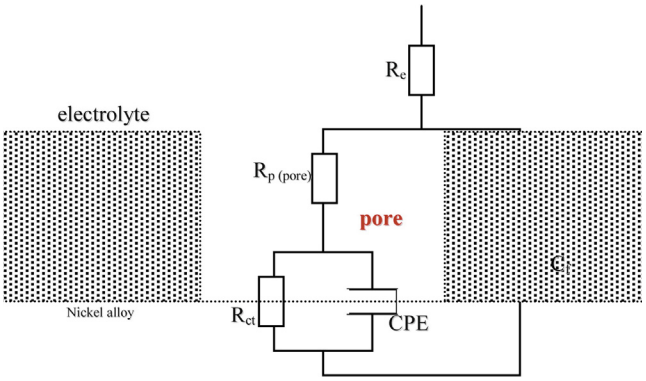

Scheme 4 Electrical equivalent circuit for the interpretation of experimental impedance diagrams of passivated alloy III at 3.0, 6.0 and 9.0 M in H_3PO_4. R_p, electrolytic resistance through the pores; C_f, film capacity; R_{ct}, charge transfer resistance; CPE, double layer capacity.

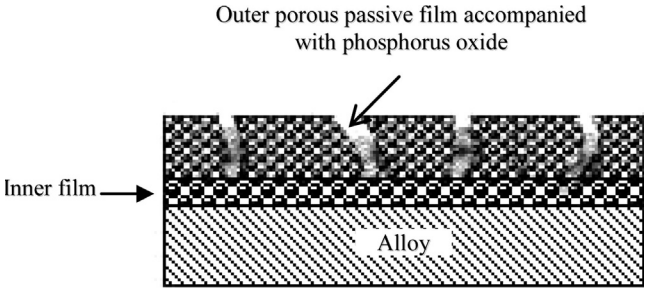

Scheme 3 Outer and Inner passive film at concentration of H_3PO_4.

3.1.2. DC electrochemical results

Potentiodynamic poloarization curves in Fig. 3a of alloy I exhibited the ability of the alloy to form protective layer in presence of PO_4^{3-}. The alloy exhibits the active–passive behavior and pseudo passivity at all examined H_3PO_4 concentrations. The active–passive behavior exhibited by the alloy may indicate a competition between the adsorption process by phosphate ions (inhibition process) and selective dissolution of Ni results in a porous passivating oxide film of low stability (I_{pass} values increase with potential). The corrosion and passivation parameters in Table 3 indicated that the I_{corr} decreases by increasing the acid concentration from 1.0 to 3.0 M as in impedance measurements. This increase in I_{corr} associated with increase markedly in I_{cc} and E_{cp} in the positive direction, increase in potential, ($E_{corr} - E_{pass}$ = 560.36 mV(SCE)), needs passivation to occur.

The corrosion potential (E_{corr}) of amorphous alloy I was (−177, −199 and −174) at 6.0, 9.0 and 12.0 M, respectively.

Appositive shift of E_{corr} values was observed for the alloy indicating better corrosion resistance. Observations of current plateau in anodic polarization curves may related to formation of non-adhering porous layer on alloy surface which may consist of soluble oxides.

Although 3.0 M H_3PO_4 delays to some extent the passivity of alloy I, there is an appearance of a relatively stable passive region at 6.0–12.0 M H_3PO_4 solutions (lower pH). The current plateau exhibited by the anodic polarization curve obtained in H_3PO_4 solution can be attributed to a non adhering porous layer of sparingly soluble Ni phosphate salt. This hypothesis is confirmed by a polarization test in which the sample surface looked grayish black and the solution returns to green.

Similar results were observed by several authors in H_3PO_4 solutions at critical concentration approximately 13.0 M for tilanium (Ti) and its alloys (Singh and Hosseini, 1993), 20 g/l for lead (Pb) and its alloys (Venugopalan, 1993), 7.0 M (Jianguo et al., 1995) and 4.0 M (Noor, 2005) for steel. The rate of reaction between the nickel base alloy and H_3PO_4 solution depends on the relative humidity on the alloy surface. At low relative humidity (higher acid concentration), hydrated nickel phosphate may be precipitated and acts as a diffusion barrier between the acid and the alloy surface, and may prevent further dissolution, while at high relative humidity, the salt becomes soluble and thus assists the corrosion process. This hypothesis was used widely to interpret the H_3PO_4 acid behavior. The decrease in the I_{pass} values with increasing PO_4^{3-} ion concentration indicates that the passive film becomes more protective and less porous specially by increasing the potential. The cathodic polarization curves shifted towards higher current density regions with [H_3PO_4] increase and hydrogen evolution is observed.

Nevertheless, it's clear from the Tafel curves in Fig. 3b that alloy II with 7% Cr shows a better passivation behavior than alloy I and H_2SO_4 (Arab et al., 2009) solutions, the soppiest tendency of R_{ct} was observed of I_{corr}, Table 3. In the first, the corrosion rate increased up to 3.0 M H_3PO_4. Farther increase in [H_3PO_4] strongly inhibit the anodic dissolution of the alloy in both the active and passive region and makes its passivation more visible. Polarization curves of samples show that the alloy is spontaneously passivated and significantly low anodic current densities irrespective of the acid concentrations is observed. The E_{corr} values shifted to more positive indicating the enhancing of oxide film formation. The lower values determined of I_{pass} and I_{cc} with large passive range (~720 mV(SCE)) suggested to produce highly stable non porous passivation oxide film. The product film may become thinner at low acid concentrations which allow acid to diffuse through the film/alloy interface (small pseudo-inductive loop observed in the Nyquist diagrams only at low concentrations of acid).

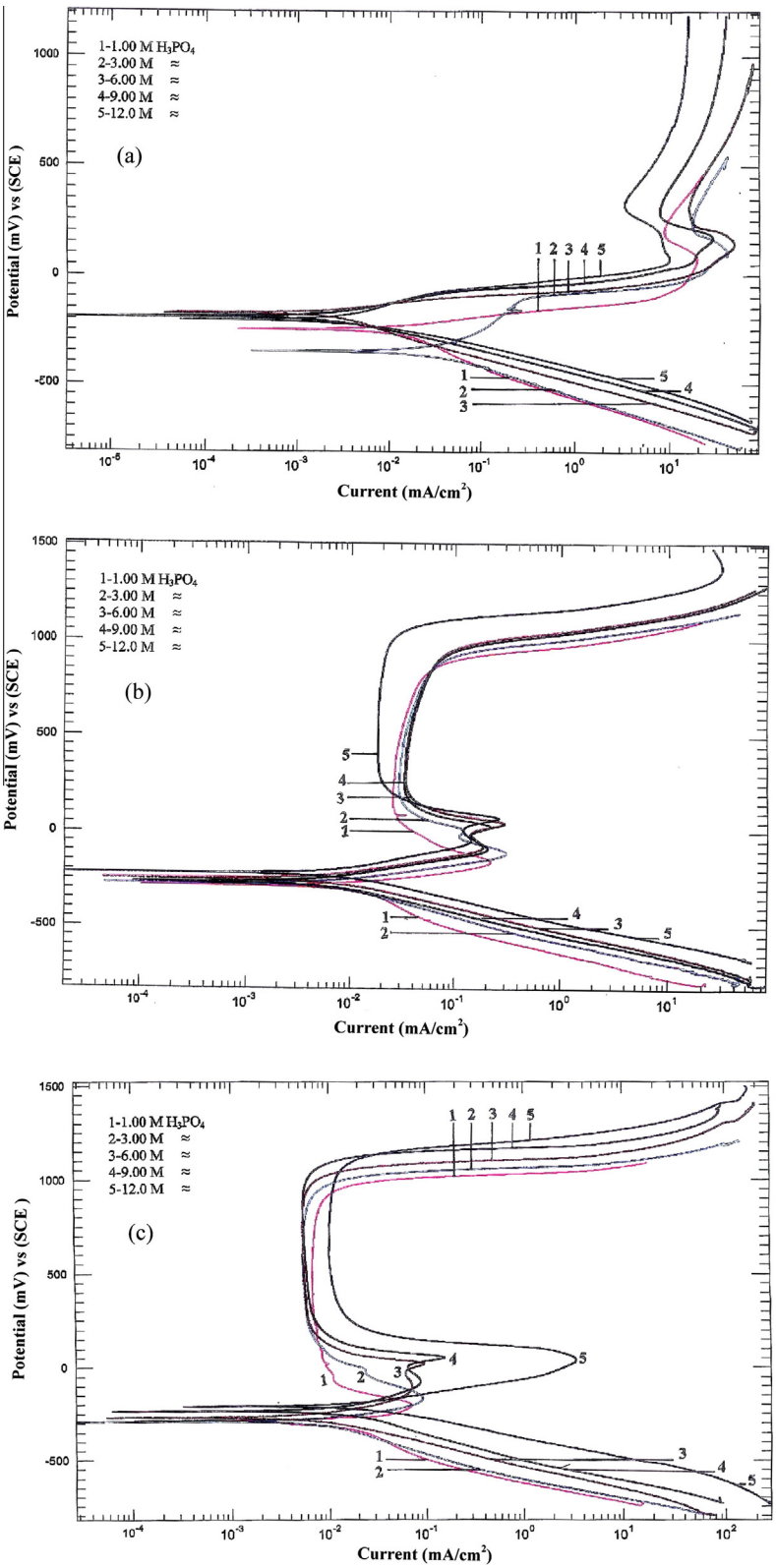

Figure 3 Potentiodynamic polarization curves of Ni-base metallic glasses alloys of different concentrations of H_3PO_4.

Two dissolution–passivation peaks were observed at anodic potentiodynamic curves (expect at 1.0 M). The first peak was attributed to form of unstable oxide layer that dissolved by potential increase. Then at high potentials another peak was observed where the stable oxide film formed lead to considerable reduction on the corrosion rate (I_{corr} values) and improved the degree of passivation (decrease I_{pass} value).

In the transpassive region a sharp increase in the current density is observed at potential 1200 mV (SCE) at 12.0 M H_3PO_4 solution and at (800–1000) mV(SCE) for other tested

Table 3 Electrochemical parameters of polarization for metallic glassy alloys in naturally aerated H_3PO_4 solutions at 30 °C.

Alloy	C (M)	$-E_{corr}$ (mV/SCE)	I_{corr} ($\times 10^2$) (mA/cm^2)	E_{cp} (mV/SCE)	E_{pass} (mV/SCE)	E_b (mV/SCE)	E_{corr}–E_{pass} (mV)	I_{cc} (mA/cm^2)	I_{pass} (mA/cm^2)
I	01.0	247	1.89	81	198	214	445	18.69	08.78
	03.0	330	2.59	114	221	263	551	38.58	17.31
	06.0	177	1.24	147	254	328	431	45.98	15.91
	09.0	199	1.19	74	275	320	474	17.56	07.82
	12.0	193	0.75	72	305	343	498	09.83	03.36
II	01.0	287	0.23	−158	92	805	379	0.29	0.029
	03.0	276	0.33	13	136	858	412	0.12	0.033
	06.0	248	0.24	48	211	928	459	0.29	0.038
	09.0	265	0.15	35	163	897	428	0.21	0.039
	12.0	217	0.14	75	277	1000	494	0.26	0.019
III	01.0	297	0.34	−203	263	803	560	0.069	0.007
	03.0	287	0.18	−167	291	812	578	0.090	0.005
	06.0	269	0.05	+23	260	893	529	0.093	0.006
	09.0	232	0.19	+54	350	971	582	0.154	0.006
	12.0	210	0.51	+38	377	1000	587	03.35	0.010

solutions. The evolution of gas on the surface was observed in the transpassive region on the outside of the formed film which suggested to be oxygen according to the following reaction:

$$4OH^- = O_2 + 2H_2O + 4\bar{e} \quad (8)$$

On the other hand, according to the Pourbaix diagram for Cr at potential higher than 1300 mV (SCE), the Cr^{3+} can be oxidized to Cr^{6+} (H_2CrO_4, CrO_4^{2-}, Cr^{6+}–$4H_2O$) to form soluble compounds (Pourbaix, 1966; Bojinov, 2003; Bojinov et al., 2000) confirm that the transpassive dissolution is a complicated process including electron and ion transport through a surface film. Multi-steps electrochemical reactions at the film/solution interface and transport of reaction products in the bulk solution is suggested. The parallel polarization curves at the different acid concentrations in transpassive region indicated that the dissolution process occurs with the same mechanism.

Secondary current plateau was observed. This may due to precipitate of phosphate oxide on the alloy. The specimens surface became gray after the polarization experiment. Chaudhary and Singh (1993) pointed out that the second passive region of Ni is due to either different type of adsorption processes on the electrode surface or oxide film transformation. Such mechanism of transformation is consistent with the assumption that Ni goes in to the solution although the passive film in the transpassive region is considered to be higher valent oxides associated with oxygen evolution. The test solution developed was light green yellowish color at the end of the experiment in each concentration of H_3PO_4 acid.

The anodic polarization curves for alloy III with 13%Cr (Fig. 3c) revealed active, passive and transpassive behavior. The maximum values of I_{corr}, I_{cc} and I_{pass} were observed for the alloy in 12.0 M H_3PO_4 in Table 3 and the minimum value of these was in 6.0 M, which is in agreement with the impedance study. Only at 6.0 M and 9.0 M H_3PO_4, two peaks were observed, the first at −74 and −85 mV (SCE) and the second at +23 and +54 mV (SCE), respectively. Stable and homogeneous adherent nonporous protective passive layer produced a good resistance behavior and highest degree of passivation (lower I_{cp} and E_{pass} value) with wider passive region ($E_b - E_{pass}$ values about 731 mV(SCE)). This is confirmed by the increase Cr presentation in alloy lead for lower value of potential needed to reach the passivity region (E_{corr}–E_{pass} values). These values are lower than in H_2SO_4 solutions (Arab et al., 2009).

The corrosion and resistivity behavior under applied potential was further examined by XPS analysis of the surface film for the studied alloys (alloy I (Cr-free), alloy II (7%Cr(and alloy III (13% Cr)) before and after impedance and polarizations measurements in 3.0 M H_3PO_4 open to air experiment at 30̊C.

XPS analysis of the alloy I surface shows that the peak binding energy of Ni^m $2p_{3/2}$ and Ni^{ox} $2p_{3/2}$ was approximately 852.8 eV. After the treatment, peak binding energy of P^{ox} $2p_{3/2}$ was approximately 135 eV as shown in Fig. 4. This value indicated the presence of phosphorus pentoxide [$(P_2O_5)_2$] on alloy surface. No change exhibited for Si $2p_{3/2}$ and B $2p_{3/2}$ before and after treatment.

These data confirmed that pseudo passivation was exhibited by the alloy I in H_3PO_4 solutions which may attributed to porous phosphorus pentoxide [$(P_2O_5)_2$].

The Ni 2p3/2 was about 852.9 eV, before and after the treatment for both alloys II and III. The Cr 2p spectrum of these two alloys give binding energy of the Cr^m $2p_{3/2}$ and Cr^{ox} $2p_{3/2}$ electrons at 574.2, 575.3 and 577.1, 576.8 eV, respectively which is in agreement with values obtained by many authors (Asami and Hashimoto, 1977; Naka et al., 1979; Hashimoto, 1983a, 1983b; Mitsuhashi et al., 1987; Zhang et al., 1992a,b; Macdonald et al., 2004; Gray et al., 2006).

On the other hand, the peak binding energy of $P2p_{3/2}$ electron was observed at 135.6 eV which indicated the formation of $(P_2O_5)_2$ on the alloys surfaces.

According to analysis, the corrosion resistance and the limiting current shown in anodic polarization curves of nickel base glassy alloys II and III are attributable mainly to the formation of hydrated chromium oxyhydroxide film [$CrO_x(OH)_{3-2x}{\cdot}nH_2O$] which formed in range 576.3–579.7 eV (Asami and Hashimoto, 1977; Naka et al., 1979; Hashimoto, 1983a, 1983b; Mitsuhashi et al., 1987; Zhang et al., 1992a,b; Macdonald et al., 2004; Gray et al., 2006).

The oxyhydroxides formation may occur due to the following reactions:

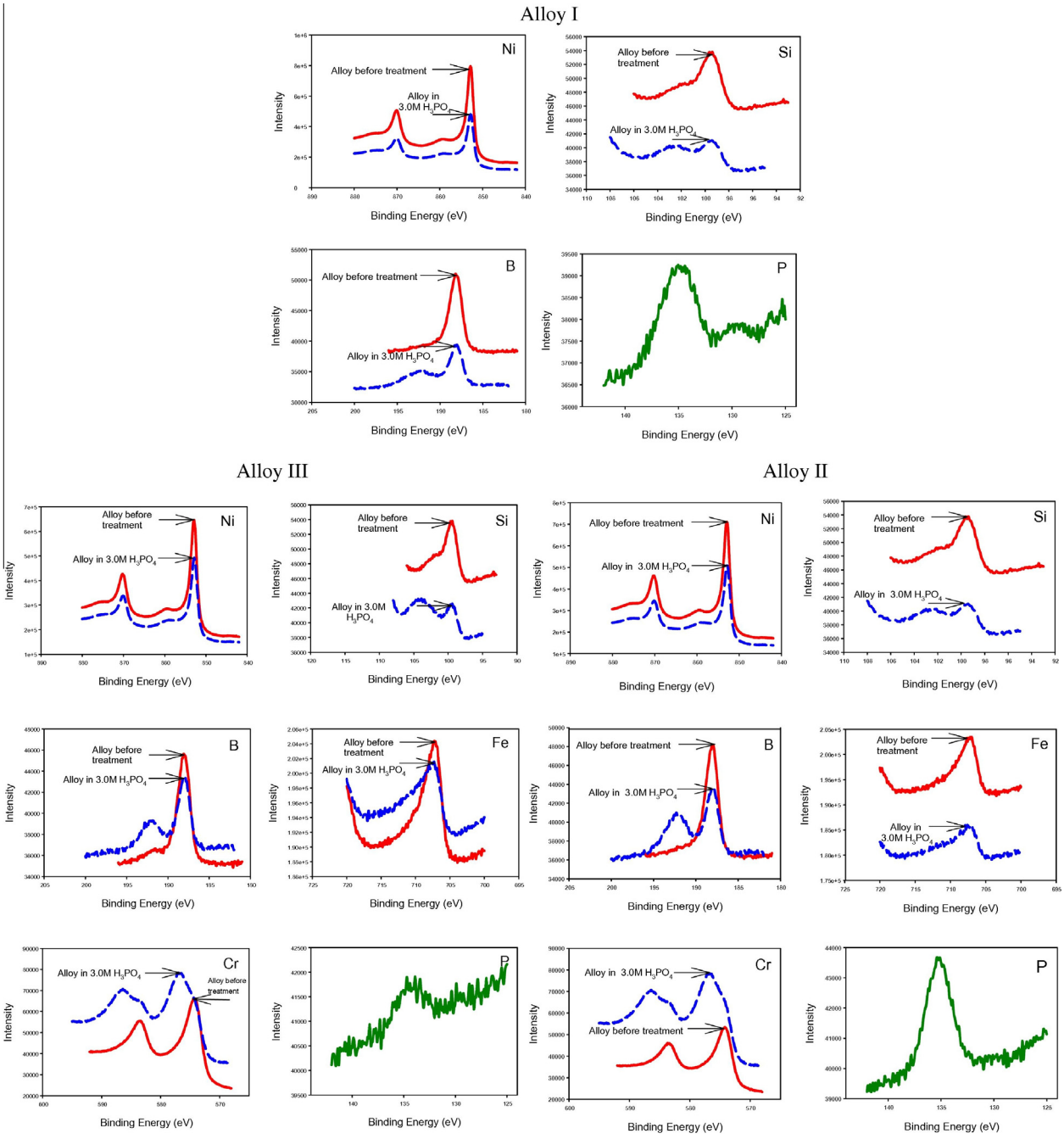

Figure 4 The photo-electron spectra obtained for the metallic glassy alloys before and after the experiment in the 3.0 M H_3PO_4 solution.

Table 4 Calculation the oxide thickness on alloy II and III from impedance data.

C (M)	Thickness of oxide (nm)	
	Alloy II	Alloy III
1.00	5.27	5.60
3.00	4.34	10.86
6.00	4.99	52.23
9.00	4.97	9.90
12.0	5.10	3.64

From Cr^{3+}

$$Cr^{3+} + 2H_2O \rightarrow CrOOH. + 3H^+ \quad (9)$$

or from $Cr(OH)_3$

$$Cr(OH)_3 + 2H_2 \rightarrow CrOOH + 3H^+ \quad (10)$$

Naka et al.(1979) reveal that the anodic activity of the FeB, CoB and NiB alloys has a dual function with respect to corrosion, depending on the chromium content of the alloy. When the chromium content of the alloy is sufficiently high to form a protective film, the high anodic activity of the alloy facilitates the active dissolution of the alloy and hence the formation of surface

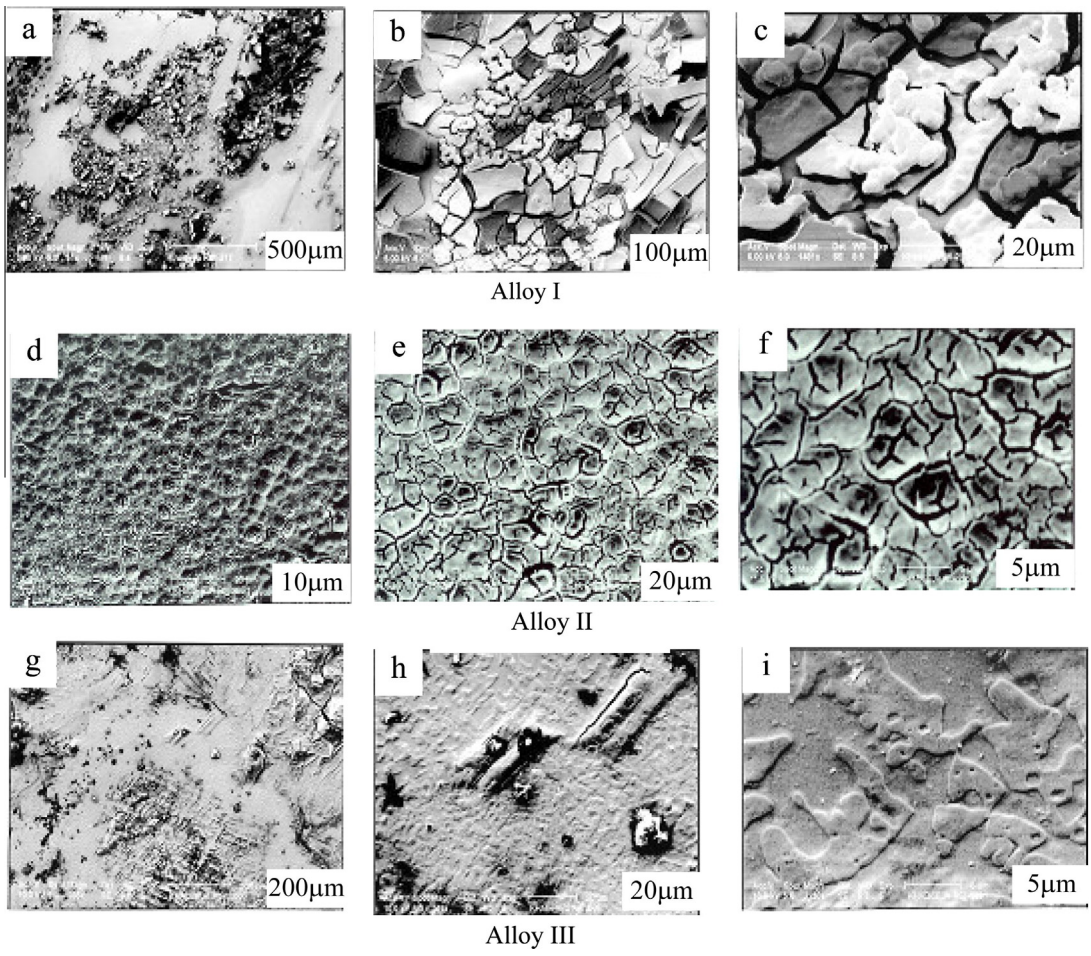

Figure 5 SEM morphology for Ni-base metallic glasses alloys at different magnifications in 3.0 M H_3PO_4.

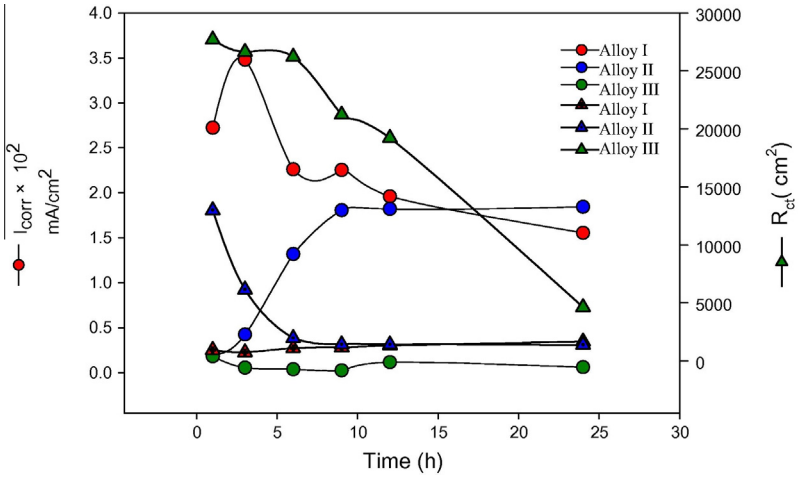

Figure 6 I_{corr} and R_{ct} variation with immersion time of Ni-base metallic glasses alloys in 3.0 M of H_3PO_4.

film in which protective species, that is, chromic ions are highly enriched. In this study, the spontaneous passivation layer formed on the alloy was the passive hydrated chromium oxyhydroxide film which is the most active for alloy III than alloy II.

The average thickness of hydrated chromium oxyhydroxide film on alloy II and III was calculated using Eq. (7), assumed ε to be 30 F m^{-1} (Hashimoto, 1983a, 1983b; Mitsuhashi et al., 1987; Zhang et al., 1992a,b; Gray et al., 2006; Hashimoto et al., 2007).

The average oxide thickness (d) values formed on alloy II and III are calculated at different concentrations of H_3PO_4 and listed in Table 4.

It is clear from Table 4, that the thickness of the oxide film is several nanometers (nm) and grows linearly with the

decrease on the acid concentration. Also the table explains the protective nature of Cr_2O_3 which is $[CrO_x(OH)_{3-2x}{\cdot}nH_2O]$ (Asami and Hashimoto, 1977). The oxide film which grows on alloy III is more thicker than that film formed on the surface in alloy II in spite of that at 12.0 M. Therefore, the overall decrease in the corrosion resistance and the increase in the capacitance for alloy II were both correlated with the decrease in the effective thickness of the oxide layer.

3.2. Scanning electron microscope (SEM)

The SEM micrographs in Fig. 5a–c show the surface of glassy alloy I in 3.0 M H_3PO_4. The bulk glassy alloy does not suffer pitting corrosion because no pit is observed on the surface of the samples after the test. Typical cracked P_4O_{10} oxide layers can be seen of the alloy surface which results in the increase in the I_{pass} values as the potential become more positive.

Fig. 5d–f show the protective passive layer of oxy-hydroxide formed on II alloy surface. Some cracks and small pits exhibit in the oxide layer are shown. This explains the reduction in the efficiencies properties of oxide layer formed at 3.0 M of acid.

Nearly compact passive layer covering most of alloy III, Fig. 5g and h. The high homogeneous oxide film reflects the high values of n in impedance study .The higher magnification, Fig. 5i shows some damage in oxide layer. These porous may the center in which O_2 evolutes in transpassive region. At high concentration the PO_3^- ions, (p_4O_{10}) may participate and, a film formation beside the first one will increase the thickness.

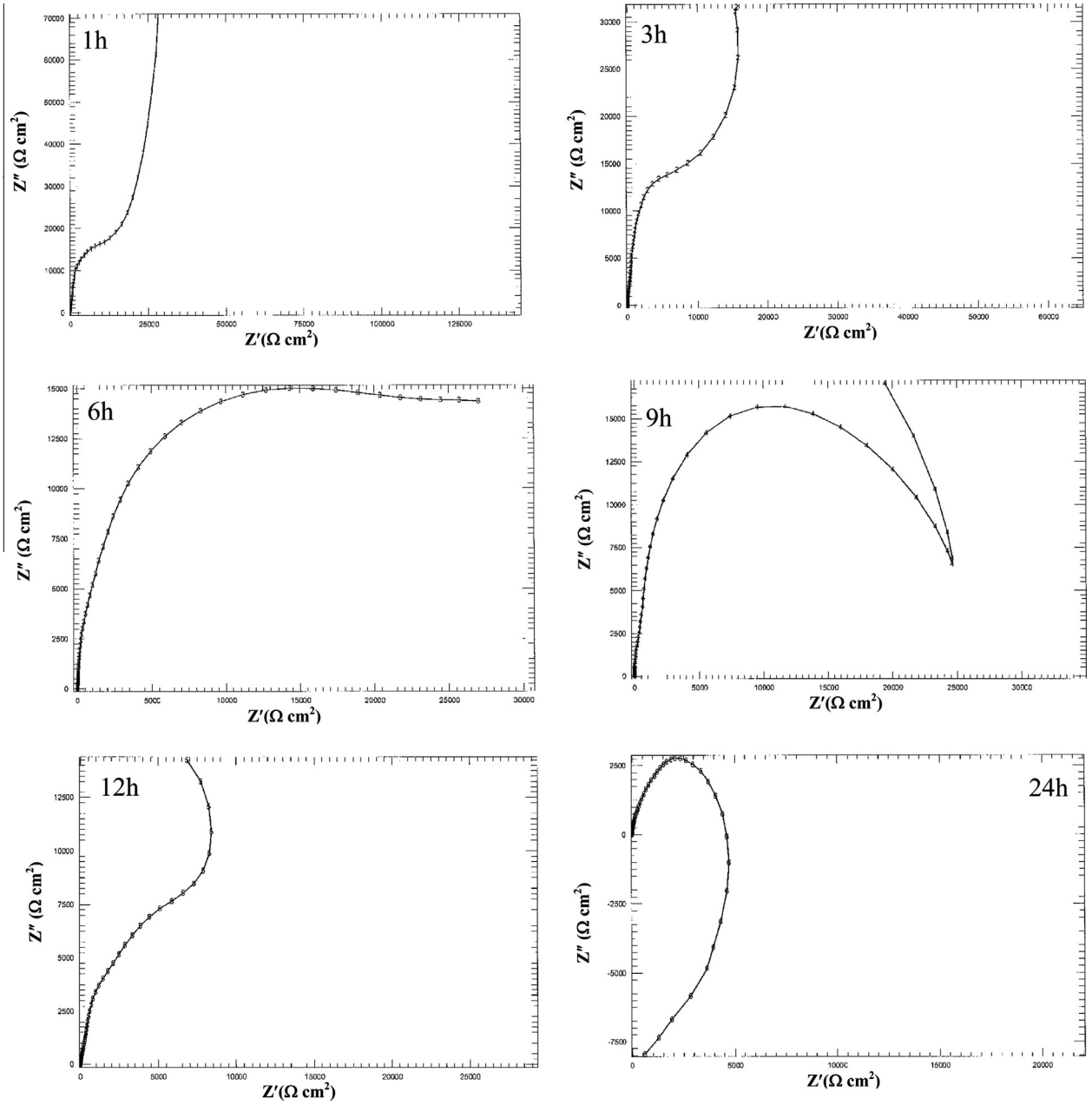

Figure 7 Impedance plots of metallic glassy alloy III measured at different immersion times in 3.0 M H_3PO_4 solution.

3.3. Immersion effect

The effect of immersion time on the electrochemical behavior of alloy I in 3.0 M H_3PO_4 acid was studied. The impedance spectra recorded for alloy I in 3.0 M H_3PO_4 solution at different immersion time (1, 3, 6, 9, 12, 24 h) is given in Fig. 6. One capacitive loop is observed irrespective of the immersion period with an open end at low frequency. The corresponding Bode-phase plots showed one time constant with Θ_{max} about 80. This reveals that there is only one reaction controlling the corrosion process. This reaction is the homogeneous corrosion of the surface in contact with the solution. The impedance of the alloy is reduced in the first 3 h of immersion. Prolonging the exposure time results an increase in the size of capacitive loop, indicating the continuous growths of the oxide layer (P_4O_{10}) and the increases in thickness. Polarization curves of alloy I reveal that there are no major differences between the general type of electrochemical behavior of the alloy in the forward and reverse polarization cases. As in the impedance measurements the I_{corr} values increase in the first 3 h. The passivation tendency and the degree of passivation of the alloy I is lower than that estimated from forward scan at all immersion times. This reveals that the reveres scan increases the corrosion tendency and the oxide formed by the reveres scan is less effective in alloy protection.

One point of additional interest in the polarization curves is the positive hysteresis observed at all immersion time. However, this is not likely to be due to pitting corrosion because of: Firstly, there is no rapid increase in the current density during the forward scan except that due to the pseudo passivation. Secondly, alloy I is usually resistant to localized corrosion in H_3PO_4 as shown in part one. Instead, the observed hysteresis is thought to be due to the selective dissolution of nickel which increases the surface area by increasing the porosity of oxide layer. This also confirms the higher values of I_{corr}.

In alloy II the Nyquist plots recorded after 1 h of immersion in 3.0 M H_3PO_4 solution has the larger value of charge transfer resistance. During the prolonging, the resistivity of the alloy for electrochemical dissolution decrease and tendency for Faradic attack appears as shown in Fig. 6. The small pseudo inductive loop present at the low frequency after 3 h, immersion indicated that the alloy prolonging in H_3PO_4 solution may formed accelerating intermedial species that may adsorbed at hydrated chromium oxy-hydroxide film causing some defects on it. As a result the thickness of the protection layer decrease. Both the upward and downward sweep shows an active–passive transition. The corrosion current density decreases gradually as the immersion time increases and reaches its maximum value after immersion of 24 h. Slight increase in I_{corr} values is observed in reveres scan. The large negative hysteresis suggests that the amorphous alloy II is better passivated after transpassive dissolution. The small positive hysteresis (corresponding to small pseudo inductive loop) seen in the transpassive region indicates that alloy II dissolves faster during the reverse scanning but it retuned faster to the passive state ($\Delta E \sim 9$ mV(SCE)).

Similar to alloy II the alloy III loses its resistivity in 3.0 M H_3PO_4 by prolonging the exposure time, Fig. 6. The most interesting phenomenon in the impedance spectra that pseudo inductive loop appears after 15 min immersion, Fig. 2e, converted to negative resistance is shown in Fig. 7. This mean that during the prolonging, the low-frequency ends are turning upwards and also to the left, and dissolution process turned to passivation process (Bentova et al., 2004; Bojinov et al., 2003). This phenomenon was observed with pure Ni in 14.8 M H_3PO_4 (Bentova, 2004) and with Nb in 5.0 M NaOH (Bojinov et al., 2003) when the impedance measurements were performed at transpassive region. The observing of negative impedance means that polarization resistance is very large. Slemnik et al. (2002, 2003) revealed that the sudden transition of metal/solution interface from a state of active dissolution to the passive state has been attributed to the formation of either a monolayer (or less) of absorbed oxygen on the surface, or to the coverage of surface by a three-dimensional corrosion product film. In either case, the reactive metal is shielded from the aqueous environment and the current drops sharply to a low value that is determined by the movement of ions or vacancies across the film. In the complex plane impedance diagram the high frequency arm of the impedance is typical of a resistive/capacitive system, but the impedance terminates in a negative differential resistance as $\omega \to 0$. At higher potentials, the high-frequency locus is again dominated by an apparent resistive/capacitive response, but the low-frequency arm is not observed to terminate at the real axis, in this case because of the very high value for the polarization resistance. The origin of the negative resistance can be accounted theoretically in terms of an increasing coverage of the surface by an absorbed intermediate as the potential is increased. Thus, the low-frequency loop exhibited is due to relaxations involving this surface species, which mean that the low– frequency response is dominated by the adsorption/passivation process.

This transition may attributed to the adsorbed corrosion product film on the oxide layer that increases the thickness of the oxide film. But the oxide thickness and the alloy resistivity decreases during the prolonging as shown in Fig. 6. The competitive process returns to appear after 24 h, of immersion. These results can be explained by considering that adsorption process, which take place on the oxide film, is strongly dependent on the immersion time. By increase of the propagation time, the adsorption process may reduced. The high values of R_{ct} even after 24 h, denote the good corrosion resistivity of alloy III in H_3PO_4 solution.

Cyclic potentiodynamic polarization curves estimated after impedance measurements at studied immersion time are shown in Fig. 8. As expected no passive region was observed with either forward nor reveres scan at any immersion time for alloy I. The absence of positive hysteresis loop indicates that the alloy does not suffer localized attack in the studied range of immersion time. Active–passive polarization behavior was observed in all curves, the alloy spontaneously passivated at low potential. Stable with wide range passive range observed in spite after 12 h, confirm the high protective properties of oxy-hydrated film. After immersion for test longer time, the passive state of the alloy becomes unstable, leading to a number of peaks and valleys. The existence of a small hysteresis loop when the potential is scanned toward the negative direction should be attributed to the dissolution in the transpassive region or due to oxygen evolution. The amorphous alloy III is better passivated after transpassive dissolution. The high

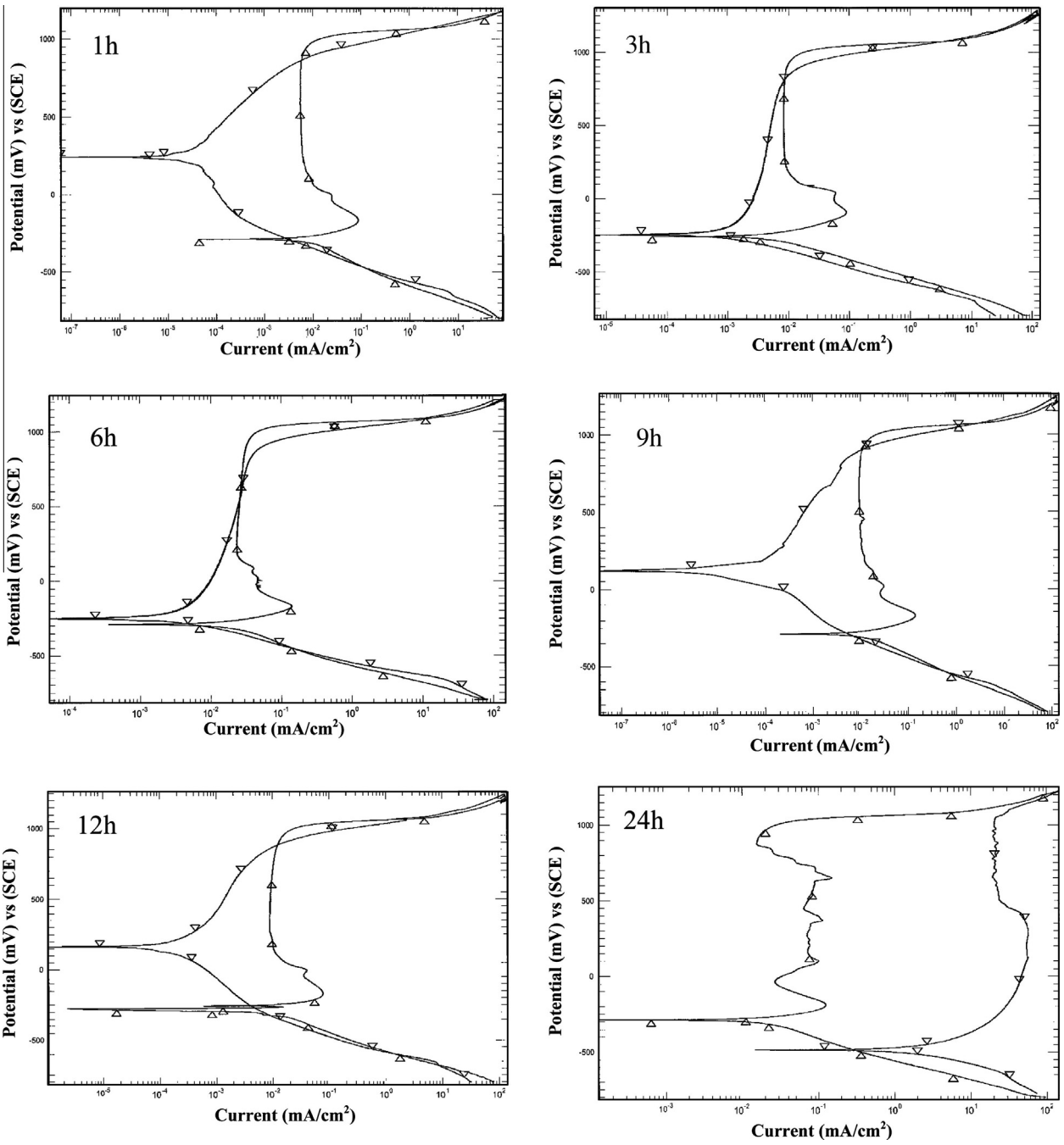

Figure 8 Forward and reveres polarization curves of metallic glassy alloy III measured at different immersion times in 3.0 M H_3PO_4 solution.

values of I_{pass} recorded after immersion for 24 h, confirmed the increase of the accelerating intermediate species process rather than the completive process.

4. Conclusion

The electrochemical behavior and passivation susceptibility of amorphous Ni(Cr)FeSiB alloys in H_3PO_4 solutions at concentrations at different immersion times were investigated. The following conclusions can be withdrawn:

1. The difference in the behavior in studied alloys ($Ni_{92.3}Si_{4.5}B_{32}$, $Ni_{82.3}Cr_7Fe_3Si_{4.5}B_{3.2}$ and $Ni_{75.5}Cr_{13}Fe_{4.2}Si_{4.5}B_{2.8}$) can be attributed to their composition.
2. Critical concentration behavior appeared in $Ni_{92.3}Si_{4.5}B_{32}$ and $Ni_{82.3}Cr_7Fe_3Si_{4.5}B_{3.2}$ alloys. Pseudo-passive and compact film formed on the alloys surface, respectively, become more effective after the translate point.
3. Passivation layer thickness formed on chromium-bearing $Ni_{75.5}Cr_{13}Fe_{4.2}Si_{4.5}B_{2.8}$ alloy decrease at high concentrations of PO_4^{3-}.

4. The lower resistance was observed for Cr-free $Ni_{92.3}Si_{4.5}B_{32}$ alloy.The passive region obtained in H_3PO_4 acid solutions are wider for $Ni_{75.5}Cr_{13}Fe_{4.2}Si_{4.5}B_{2.8}$ than those obtained in Ni82,3Cr7Fe3Si4.5B3.2 alloy.
5. XPS analysis confirmed that growth of phosphorus pentoxide (P_4O_{10}) layer on alloy I surface resulting in the pseudo passivation of it. Hydrated chromium oxyhydroxide layer causes the chromium-bearing alloys resistance.
6. Beneficial effect of Cr for corrosion resistance was observed clearly from the thickness values of hydrated chromium oxyhydroxide layer calculated at different concentrations of acid.
7. Increasing the dissolution resistance of the alloy III, may due to the filling the pores in the outer layer resulting in improvement of the passive state and decrease in Q values and corrosion rate mm/y.
8. The low CPE (Q) values in the case of alloy III reflex the high capacitive behavior of the alloy surface and thicker oxide layer on this alloy compared with alloy II.
9. The effect of immersion time on the electrochemical behavior and passive layer characteristics was studied.

Acknowledgements

The authors wish to express their gratitude to Dr.Hartmann Thomas from Vacuumschmelze company for supplying the nickel base alloys of this research and to Kink Abdulaziz City of Science and Technology (KACST) for supporting this study under postgraduate project (GSP-14-105).

References

Arab, S.T., Emran, K.M., 2009. Chem. Phys. News 50, 130.
Arab, S.T., Emran, K.M., Al-Turaif, H.A., 2009. J. Korean Chem. Soc. 53, 281.
Asami, K., Hashimoto, K., 1977. Corros. Sci. 17, 559.
Asami, K., Hashimoto, K., Masumoto, T., Shimodaira, S., 1976. Corros. Sci. 16, 909.
Bentova, I., Bojinov, M., Tzvetkoff, T., 2004. Electrochim. Acta 49, 2295.
Bojinov, M., 2003. T. Tzvetkoff J. Phys. Chem. 107, 5101.
Bojinov, M., Fabricius, G., Kinnunen, P., Laitinen, T., Makela, K., Saario, T., Sundholm, G., 2000. Electrochim. Acta 45, 2791.
Bojinov, M., Cattarin, S., Musiani, M., Tribollet, B., 2003. Electrochim. Acta 48, 4107.
Chaudhary, R.S., Singh, A., 1993. Br. Corros. J. 28, 277.
Chen, Y., Hong, T., Gopal, M., Jepson, W.P., 2000. Corros. Sci. 42, 979.
Gray, J.J., El Dasher, B.S., Orme, C.A., 2006. Surf. Sci. 600, 2488.
Hashimoto, K., 1983. Passivity of metals and semiconductors. In: Froment, M. (Ed.), Proceedings of 5th International Symposium Passivity. Elsevier, Amsterdam, p. 247.
Hashimoto, K., 1983. Passivity of Metals and Semiconductors. In: Froment, M. (Ed.), Proceedings of 5th International Symposium Passivity. Elsevier, Amsterdam, p. 235.
Hashimoto, K., Asami, K., Kawashima, A., Habazaki, H., Akiyama, E., 2007. Corros. Sci. 49, 42.
< http://en.wikipedia.org/wiki/Passivation > .
Inoue, A., 1998. Bulk Amorphous Alloys: Practical Characteristics and Applications. Trans Tech Publications Inc., MI, Switzerland.
Jianguo, Y., Lin, W., Otieno-Alego, V., Schweinsberg, D.P., 1995. Corros. Sci. 37 (6), 975.
Johnson, W.L., 1999. Bulk Glass Forming Metallic Alloys: Science and Technology. MRS Bull, MI, America.
Katagiri, H., Meguro, S., Yamasaki, M., Habazaki, H., Sato, T., Kawashima, A., Asami, K., Hashimoto, K., 2001. Corros. Sci. 43, 171.
Kawashima, A., Asmi, K., Hashimoto, K., 1984. Corros. Sci. 24 (9), 807.44.
Lee, H.J., Akiyama, E., Habazaki, H., Kawashima, A., Asami, K., Hashimoto, K., 1997. Corros. Sci. 39 (2), 32188.
Macdonald, J.R., Johanson, W.B., 1987. In: Macdonald, J.R. (Ed.), Theory in Impedance Spectroscopy. John Wiley & Sons, New York.
Macdonald, D.D., Sun, A., Priyantha, N., Jayaweera, P., 2004. J. Electroanal. Chem. 572, 421.
Mitsuhashi, A., Asami, K., Kawashima, A., Hashimoto, K., 1987. Corros. Sci. 27, 957.
Naka, M., Hashimoto, K., Masumoto, T., 1979. J. Non-Cryst. Solids 34, 257.
Noor, E.A., 2005. Corros. Sci. 47, 33.
Oelhafen, P., Liard, M., Güntherodt, H.J., Berresheim, K., Polaschegg, H.D., 1979. Solid State Commun. 30 (10), 641.
Pourbaix, M., 1966. Atlas of Electrochemical Equilibria in Aqueous Solutions. Pergamon Press Inc., New York.
Qin, C., Asami, K., Kimura, H., Zhang, W., Inoue, A., 2010a. Electrochim. Acta 54 (5), 1612.
Qin, C.L., Zeng, Y.Q., Louzguine, D.V., Nishiyama, N., Inoue, A., 2010b. J. Alloys and Comp. 504, 172.
Salimon, A.I., Ashby, M.F., Bréchet, Y., Greer, A.L., 2004. Mater. Sci. Eng. 375–377, 385.
Singh, V.B., Hosseini, S.M.A., 1993. Corros. Sci. 34, 1723.
Slemnik, M., Dolecek, V., Gaberscek, M., 2002. Acta Chim. Slov. 49, 613.
Slemnik, M., Dolecek, V., Gaberscek, M., 2003. Acta Chim. Slov. 50, 43.
Venugopalan, S., 1993. J. Power Sour. 46, 1.
Wu, Y., Nagase, T., Umakoshi, Y., 2006. J. Non-Cryst. Solids 352 (28–29 (15)), 3015.
Zhang, B.P., Habazaki, H., Kawashima, A., Asami, K., Hashimoto, K., 1992a. Corros. Sci. 33 (5), 667.
Zhang, B.P., Habazaki, H., Kawashima, A., Asami, K., Hashimoto, K., 1992b. Corros. Sci. 33 (10), 1519.